

## Supplemental Data

### Using a Compound Gain Field

#### to Compute a Reach Plan

Steve W.C. Chang, Charalampos Papadimitriou, and Lawrence H. Snyder

## Supplemental Results and Discussion

### The Degree of Correlation Between Eye and Hand Gain Fields

The slopes of the regressions in Figure 3 are close to but significantly smaller than -1 (all  $p < 0.05$ , linear regression). The gain field measurements might show deviations from having a slope of negative one because the gain fields are truly not perfectly correlated, because the measurement is contaminated by noise, or because of a combination of these two effects. Our regressions were type II (that is, the regression model assumed that there was uncertainty in the measurements of the values on both the  $x$  and  $y$  axes), and so noise would decrease the correlation but not systematically change the slope. Therefore the fact that the slopes were significantly different from minus one indicates that eye gain field strengths were stronger than hand gain field strengths at the population level. This may be because there are two separate populations of cells, one with matched gain fields and one with eye gain fields greater than hand (or perhaps even entirely lacking in hand gain fields). Alternatively, all cells may have slightly larger eye than hand gain fields. Our data do not allow us to make this distinction (but see legend of Supplemental Figure 5). To test whether measurement noise might also contribute to the fact that regression slopes were different from negative one, we plotted the distance of each point from the negative unity line as a function of spike-variance explained (Supplemental

Figure 5). Indeed, cells with high spike-variance explained all lay close to the negative unity line, while cells far from the line had low spike-variance explained. The 10% of cells with the highest spike-variance explained fell within the bottom 35% of deviations from the negative unity line, while the 10% of cells with the largest deviations from the negative unity line fell within the bottom 46% of spike-variance explained. Therefore we believe that measurement noise also plays a role in lowering the correlation between eye and hand position gain fields.

### **Linear Versus Multiplicative Combination of Eye and Hand Gain Fields**

If gain fields combine multiplicatively instead of linearly (Equation 3 versus Equation 1, Experimental Procedures), then negatively correlated eye and hand gain fields would not form a single gain field encoding the signed distance between the fixation point and the hand (see Equation 4). If the point of gaze is far from the hand, then the effects are moderate, e.g., a 33% difference in predicted activity between an additive and a multiplicative model for an eye-hand distance of  $50^\circ$  of visual angle (based on the median 2.30%/deg distance gain field found in the present study). However, for the eye-hand distances used in the current study ( $7.5^\circ$  and  $15^\circ$ ), the difference between the additive and multiplicative models would be only 1% or 3%, respectively. Such a small effect would be buried in the measurement noise. Future experiments could help refine the model by using much larger separations between initial eye and hand position, establishing whether the interaction between eye and hand position gain fields is strictly linear (and therefore forms a perfect eye-hand distance gain field) or involves a non-linearity such as a multiplicative term (and therefore diverges from an eye-hand distance gain field for large peripheral eye or hand positions).

## **Further Characterization of Eye and Hand Gain Fields**

Ideally, we would use more than three initial eye and hand positions in order to more precisely determine the shape of eye and hand position gain fields, and we would test for gain field interactions in all three dimensions. We suspect that, as in LIP, the gain fields of many but not all PRR neurons would be well fit by a linear function (e.g., Andersen and Mountcastle, 1983; Brotchie et al., 1995), and that gain fields will be present in multiple dimensions (Andersen et al., 1990), including the depth dimension. It would be particularly interesting to know whether the finding of equal magnitude but opposite directions of eye and hand gain fields applies across all three dimensions, and whether the *shape* of eye and hand gain fields are also matched. Because of the complexities of separating gain field effects from tuning curve shifts in multiple dimensions, these experiments will likely require chronically implanted electrode arrays from which very large data sets can be collected (Batista et al., 2007).

## **Supplemental Experimental Procedures**

### **General Recording Procedures**

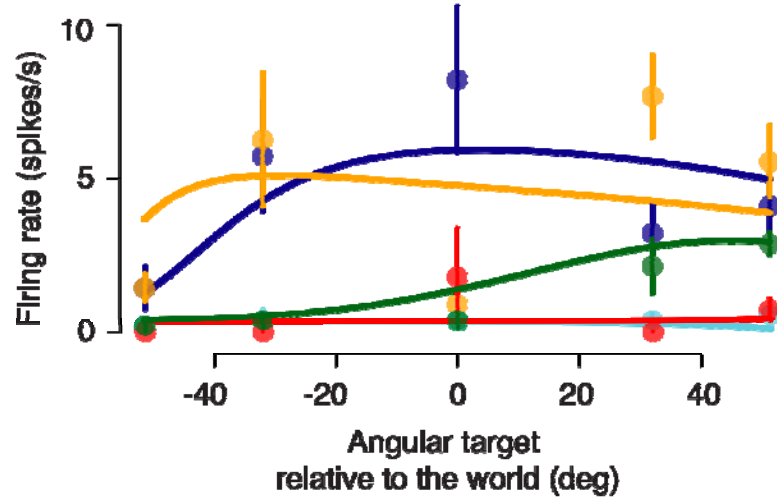
Eye position was monitored by the scleral search coil technique (CNC Engineering, Seattle, Washington). Hand position was monitored by a 13.2 x 13.2 cm custom-built touch panel that uses finely spaced (3 mm) horizontal and vertical infrared beams, 1-3 mm above a smooth surface (temporal resolution = 2 ms). A registered touch or release was defined as an incidence when a finger or fingers (typically an index finger or index and middle fingers together) broke the beams at a particular location(s) on the touch panel. The animals sat in a custom-designed monkey chair (Crist Instrument, Hagerstown, Maryland) with a fully open front

to provide unimpaired reaching movements. Visual stimuli were back-projected by a CRT projector onto the touch surface, which was mounted vertically, 25 cm in front of the animal. The recording room was sound-attenuating and light-proof, such that a dark-adapted human could detect no light when the projector was turned on but projecting no targets.

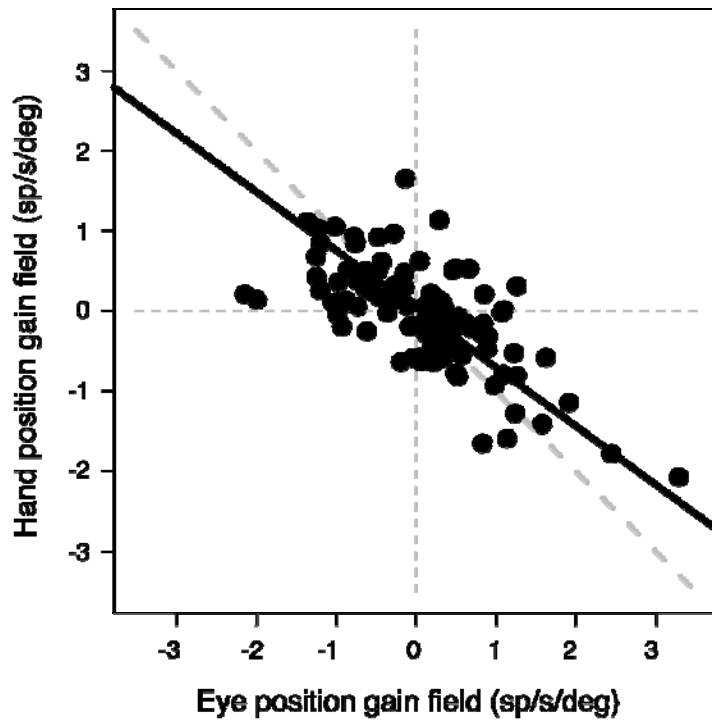
The touch screen was mounted such that the center was approximately aligned the line of sight when the eyes were estimated to be in primary position. The screen center then formed the origin of our coordinate system for measuring eye and hand position. All measurements are therefore in screen coordinates, i.e., the location at which gaze intercepts the screen, and the location at which the animal touches the screen. As a shorthand, we refer to these measurements throughout the text as eye and hand position, respectively.

We recorded neurons from two monkeys (*Macaca mulatta*). Extracellular recordings were made using glass-coated tungsten electrodes (Alpha Omega, Alpharetta, Georgia). Cells were recorded from the right hemisphere from monkey G and left hemisphere from monkey S, with each animal using its contralateral limb. For each signal we encountered, we used the mapping task to ascertain isolation, stability and the approximate preferred direction of that cell. For each stable, well-isolated single neuron that showed clear spatial tuning in the mapping task ( $n = 259$ ), we ascertained the preferred direction from the mapping task and then ran the gain field task (below). These 259 cells represented about 60% of the ~450 signals we encountered. About 30% of the signals were rejected because of poor isolation or stability, and the remaining 10% were rejected because spatial tuning was absent or unclear. In this report we analyze the data of every one of the 259 cells in which we decided to run the gain field task. Because the decision to run or not run this task in a given cell was based solely on the results of the mapping task, the only bias in cell selection was in favor of cells with spatial tuning.

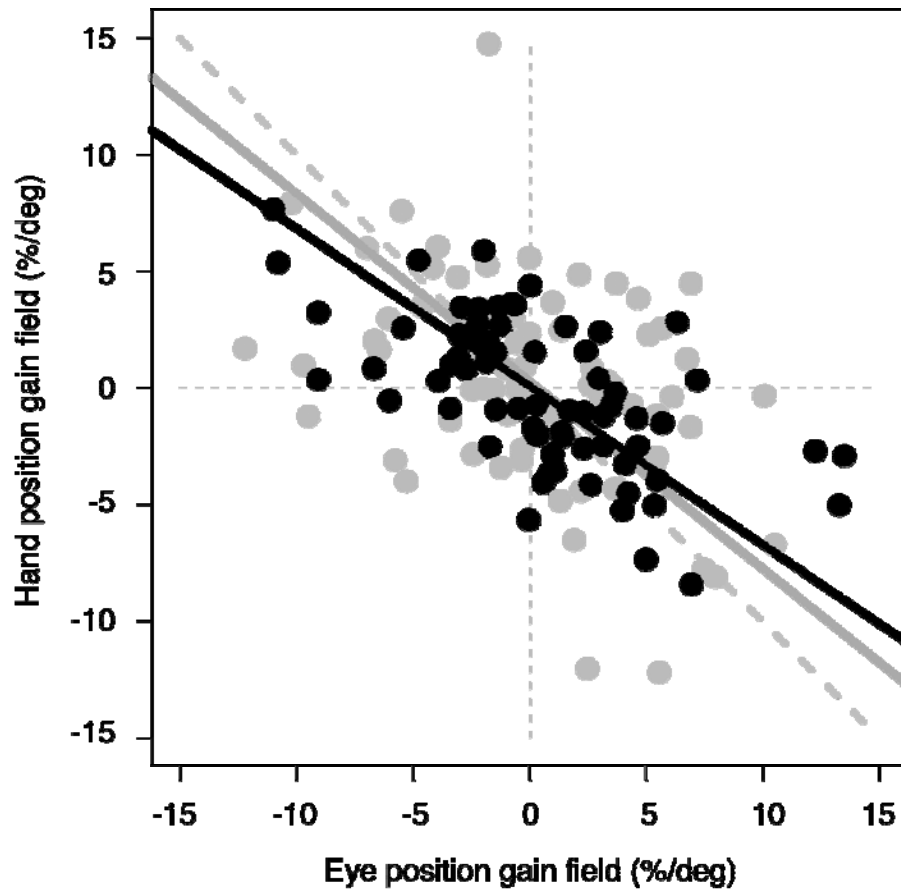
In order to guide the placement of our recording tracks and localize recording sites, we acquired high-resolution magnetic resonance images (MRI) of monkeys' brains with an MR lucent "phantom" in the recording chamber, using methods described elsewhere (Calton et al., 2002; Chang et al., 2008; Kalwani et al., 2009). Localization was accurate to within 1 mm, as determined by injecting and then visualizing MR-lucent manganese in the brain in several sessions. PRR cells straddle the boundary between MIP and V6A. A more precise anatomical label in terms of cortical areas or cortical topography is problematic. The boundaries of cortical areas in and around IPS are highly variable (Lewis and Van Essen, 2000a; Lewis and Van Essen, 2000b), and as can be seen from Figure 1C, the IPS and POS sulci are not discrete, but merge into one another. Thus the term parietal reach region emphasizes that this region is functionally defined, not anatomically defined (Snyder et al., 1997; Buneo et al., 2002; Chang et al., 2008).



Supplemental Figure 1, Chang.Supp1.pdf

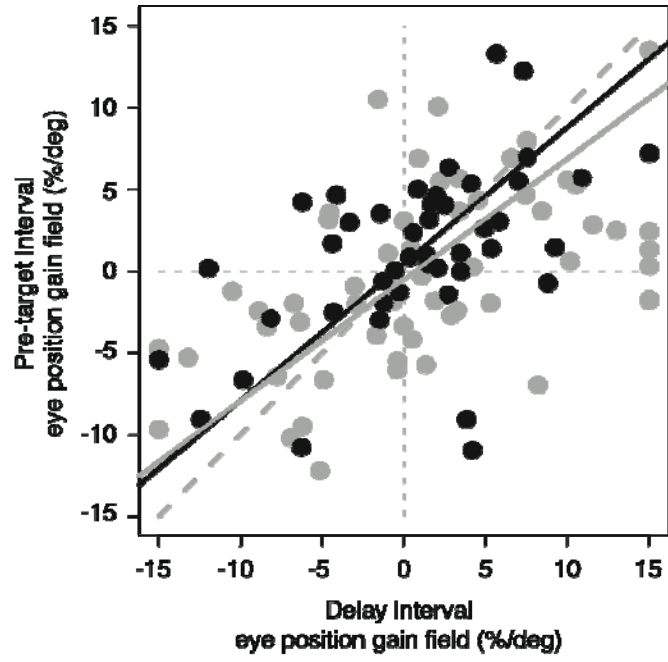


Supplemental Figure 2, Chang.Supp2.pdf

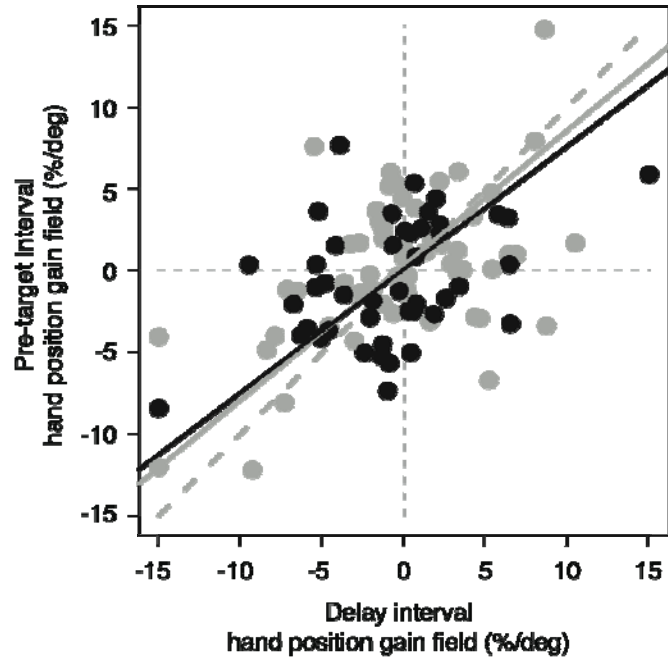


Supplemental Figure 3, Chang.Supp3.pdf

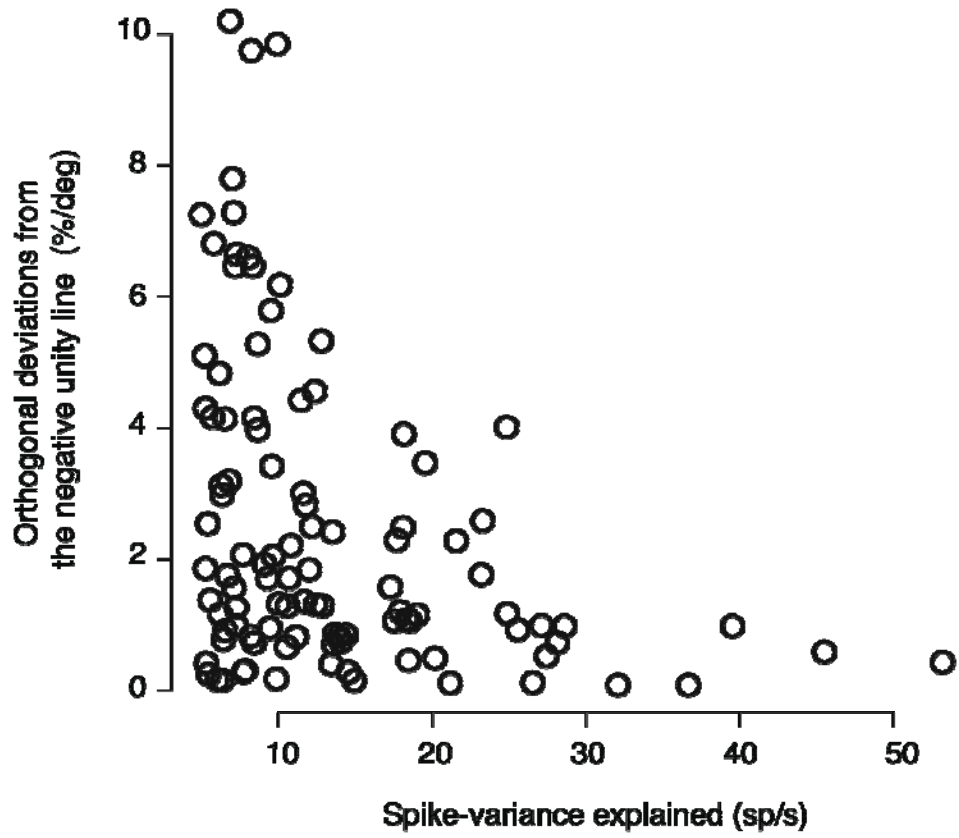
**A**



**B**



**Supplemental Figure 4, Chang.Supp4.pdf**



**Supplemental Figure 5, Chang.Supp5.pdf**

## Supplemental Figure Legends

### **Supplemental Figure 1. A Neuron with High Variance Explained, but Low Spike-Variance Explained.**

The full model explains 66% of the variance in firing rate, passing our 50% criterion. However, the modelled Gaussian modulation is only 2.6 sp/s, so that spike-variance is only 1.7 sp/s, failing both our 5 and 2 sp/s spike-variance explained criteria. Interestingly, the eye and gain fields were still similar in strength but opposite in sign (*Eyes Left* [cyan]: peak 0.54 0.26 sp/s, *Eyes Right* [dark blue]: 8.21 2.38 sp/s, *Hand Left* [yellow-orange]: 7.68 1.35 sp/s, *Hand Right* [red]: 1.79 1.59 sp/s; eye gain field: 0.39 sp/s per deg, hand gain field: -0.28 sp/s per deg). Format as in Fig. 2B.

### **Supplemental Figure 2. Negatively Coupled Eye and Hand Position Gain Fields Plotted Using Absolute Firing Rates.**

The same data as in Figure 3A but without normalization (spikes/s/deg instead of %/deg). The solid black line represents the type II regression. We normalized by dividing absolute eye and hand gain fields by the same value (delay period firing rate for a reach in the preferred direction starting from the aligned condition). This normalization has minimal effect on the population statistics. The normalized gain field data have a correlation coefficient of -0.61 ( $p < 0.00001$ , Spearman's rank correlation) and a type II regression slope of -0.74, while the unnormalized (absolute) data have a correlation coefficient of -0.67 ( $p < 0.00001$ ) and a type II regression slope of -0.73.

### **Supplemental Figure 3. The Distance Gain Field does not Require a Target.**

The negative correlation between eye and hand position gain fields is present prior to the onset of a final reach target but after the acquisition of the initial eye and hand targets. Cells with at least 2 sp/s spike-variance explained are shown in grey; cells with at least 5 sp/s spike-variance explained are shown in black. Format otherwise similar to Figure 3A.

### **Supplemental Figure 4. Eye and Hand Gain Fields are Correlated Before and After the Onset of a Reach Target.**

(A) The positive correlation between eye position gain fields before the onset of a reach target (pre-target interval) and after the onset of a reach target (delay interval). Cells with at least 2 sp/s spike-variance explained are shown in grey (Spearman's rank correlation,  $r = 0.52$ ,  $p < 0.00001$ ,  $n = 104$ ), and cells with at least 5 sp/s spike-variance explained are shown in black ( $r = 0.50$ ,  $p < 0.001$ ,  $n = 45$ ) (data points and type II regression slopes are shown). Format otherwise similar to Figure 3A.

(B) The positive correlation between hand position gain fields before the onset of a reach target (pre-target interval) and after the onset of a reach target (delay interval). Cells with at least 2 sp/s spike-variance explained are shown in grey ( $r = 0.38$ ,  $p < 0.0001$ ,  $n = 104$ ), and cells with at least 5 sp/s spike-variance explained are shown in black ( $r = 0.38$ ,  $p < 0.05$ ,  $n = 45$ ). Same format as in (A).

**Supplemental Figure 5. The Evidence for a Distance Gain Field is Stronger for Cells Whose Activity is Well Explained by the Model.**

A scatter plot of the orthogonal deviation from the negative unity line (%/deg) from Figure 3A (eye versus hand gain fields) plotted as a function of the spike-variance explained by the full model. Neurons that are well fit by the model (on the right side of the plot) are close to the negative unity line and therefore have amplitude-matched gain field strengths. Neurons that lie far from the line and therefore have eye and hand gain fields that are not matched are poorly fit by the model. Since the model allows eye and hand gain fields to vary independently, the poor fit of cells that lie far from the unity line suggests that there is not a separate, well-behaved population of eye-only gain field cells, but rather either that the data obtained from these cells that appear to be eye-only gain field cells was substantially degraded by noise, or else that the data from these cells would be better fit by a different model than the one we used.

## Supplemental References

Andersen, R. A., Bracewell, R. M., Barash, S., Gnadt, J. W., and Fogassi, L. (1990). Eye position effects on visual, memory, and saccade-related activity in areas LIP and 7a of macaque. *J Neurosci* 10, 1176-1196.

Andersen, R. A., and Mountcastle, V. B. (1983). The influence of the angle of gaze upon the excitability of the light-sensitive neurons of the posterior parietal cortex. *J Neurosci* 3, 532-548.

Batista, A. P., Santhanam, G., Yu, B. M., Ryu, S. I., Afshar, A., and Shenoy, K. V. (2007). Reference frames for reach planning in macaque dorsal premotor cortex. *J Neurophysiol* 98, 966-983.

Brotchie, P. R., Andersen, R. A., Snyder, L. H., and Goodman, S. J. (1995). Head position signals used by parietal neurons to encode locations of visual stimuli. *Nature* 375, 232-235.

Buneo, C. A., Jarvis, M. R., Batista, A. P., and Andersen, R. A. (2002). Direct visuomotor transformations for reaching. *Nature* 416, 632-636.

Calton, J. L., Dickinson, A. R., and Snyder, L. H. (2002). Non-spatial, motor-specific activation in posterior parietal cortex. *Nat Neurosci* 5, 580-588.

Chang, S. W., Dickinson, A. R., and Snyder, L. H. (2008). Limb-specific representation for reaching in the posterior parietal cortex. *J Neurosci* 28, 6128-6140.

Kalwani, R. M., Bloy, L., Elliott, M. A., and Gold, J. I. (2009). A method for localizing microelectrode trajectories in the macaque brain using MRI. *J Neurosci Methods* 176, 104-111.

Lewis, J. W., and Van Essen, D. C. (2000a). Mapping of architectonic subdivisions in the macaque monkey, with emphasis on parieto-occipital cortex. *J Comp Neurol* 428, 79-111.

Lewis, J. W., and Van Essen, D. C. (2000b). Corticocortical connections of visual, sensorimotor, and multimodal processing areas in the parietal lobe of the macaque monkey. *J Comp Neurol* 428, 112-137.

Snyder, L. H., Batista, A. P., and Andersen, R. A. (1997). Coding of intention in the posterior parietal cortex. *Nature* 386, 167-170.